Contract No:

This document was prepared in conjunction with work accomplished under Contract No. DE-AC09-08SR22470 with the U.S. Department of Energy (DOE) Office of Environmental Management (EM).

Disclaimer:

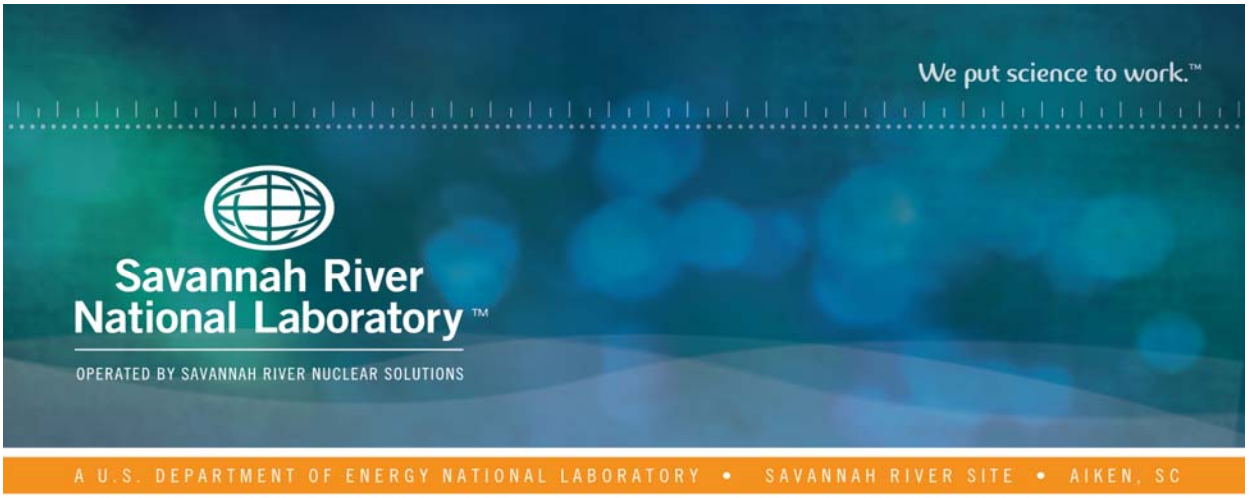

Comparison of HLW Glass Melting Rate Between Frit and Glass Forming Chemicals Using X-Ray Computed Tomography

F.C. Johnson
A.S. Choi
D.H. Miller
D.M. Immel

April 2015
SRNL-STI-2014-00562, Revision 0

DISCLAIMER

Printed in the United States of America

Prepared for
U.S. Department of Energy – Office of River Protection

SRNL-STI-2014-00562
Revision 0

Keywords: *Melting Rate, X-ray Computed Tomography, HLW, WTP*

Retention: *Permanent*

Comparison of HLW Glass Melting Rate Between Frit and Glass Forming Chemicals Using X-Ray Computed Tomography

F.C. Johnson
A.S. Choi
D.H. Miller
D.M. Immel

April 2015

Prepared for the U.S. Department of Energy – Office of River Protections under IEWO M0SRV00101

Savannah River National Laboratory™
OPERATED BY SAVANNAH RIVER NUCLEAR SOLUTIONS

REVIEWS AND APPROVALS

AUTHORS:

Signature on file
F.C. Johnson, Process Technology Programs

Signature on file
A.S. Choi, Process Technology Programs

Signature on file
D.H. Miller, Engineering Process Development

Signature on file
D.M. Immel, Imaging and Radiation Systems

TECHNICAL REVIEW:

Signature on file
D.H. McGuire for D.K. Peeler, Process Technology Programs, Reviewed per E7 2.60

Signature on file
K.M. Fox, Engineering Process Development, Reviewed per E7 2.60

APPROVAL:

Signature on file
C.C. Herman, Manager
SRNL Hanford Programs

Signature on file
S.L. Marra, Manager
Environmental & Chemical Process Technology Research Programs

ACKNOWLEDGEMENTS

The authors thank the following colleagues for their contribution to this work: Phyllis Workman and Katie Hill for the frit fabrication and melter feed preparation, and Whitney Riley, Beverly Wall, and Kim Wyszynski for sample analysis. Funding for this work was provided by the Department of Energy's Waste Treatment & Immobilization Plant Project of the Office of River Protection through Inter-Entity Work Order M0SRV00101 as managed by Albert A. Kruger is greatly appreciated.

EXECUTIVE SUMMARY

Efforts are being made to increase the loading of Hanford tank wastes in glass while meeting melter lifetime expectancies, as well as requirements for processing, regulatory compliance, and product quality. To achieve these goals, the Department of Energy – Office of River Protection (DOE-ORP) has requested that the Savannah River National Laboratory (SRNL) support the advancement of glass formulations and process control strategies in various key technical areas, which include melting rate studies. Numerous parameters influence cold cap melting and it is important to identify laboratory test methods to discern changes in melting rate. One of the primary screening tools being used at SRNL for melting rate comparisons is the dry-fed melt rate furnace (MRF). The MRF has been very effective in ranking relative melting rates of candidate frits for the Defense Waste Processing Facility (DWPF) on the laboratory-scale, which has successfully translated to facility operations.

The objective of this preliminary melting rate task was to assess the impact of frit and glass forming chemicals (GFCs) on melting rate when blended with a DWPF simulated Sludge Batch 6 (SB6) nitric-glycolic acid Sludge Receipt and Adjustment Tank (SRAT) product targeting a 1.4M Na^+ wash endpoint. The glass additive compositions and waste loadings (WLs) were defined by the Pacific Northwest National Laboratory (PNNL) 2009 and 2013 algorithms. The 2009 algorithms yielded a high boron (low alkali) additive with a WL of 35.09% and the 2013 algorithms yielded a low boron (high alkali) additive with a WL of 39.22%. A total of 4 bench-scale melting rate tests were performed with the MRF and each resulting sample beaker was analyzed with X-ray computed tomography (CT) in order to quantitatively analyze the morphology of heat treated samples and enable relative melting rate rankings. The following observations and conclusions were drawn from the results provided in this report:

- *High boron (low alkali) melter feed* - There are minimal or no differences between the melting rates of frit and GFCs.

- *Low boron (high alkali) melter feed* - The melting rate for the frit based melter feed is slightly higher than GFCs, which is most likely due to the additional CO_2 generation from the decomposition of Na_2CO_3 in the GFCs during melting.

- The evolution of excess CO_2 from the GFCs increases the total (calculated) gas evolution from the high and low boron feeds by 5% and 11% above those from the frit-based counterparts, respectively.

- The low boron feeds melted faster than their high boron counterparts (despite the fact that the low boron melter feeds were based on a higher WL), which is likely due to the higher total sodium content (~64% more than the high boron feeds).

- The primary advantages of the X-ray CT technique are that it (i) eliminates subjectivity that was associated with the previous visual method, (ii) enables quantification of materials in varying stages of melting along with the radial and vertical distribution of voids and bubbles, and (iii) allows for the entire volume of the sample to be analyzed as opposed to a 2D image of a particular cross-section, which may not be the most representative view of the entire sample.

Once the pellet tests at PNNL have been completed, a thorough review of the data will be performed to determine if the results can be compared or provide complementary insight into the melting behavior of these different melter feeds. Based on the results of this study, other parameters influencing melting rate could also be studied using melter feeds that are more representative of WTP.

TABLE OF CONTENTS

LIST OF TABLES

LIST OF FIGURES

LIST OF ABBREVIATIONS

2D	two-dimensional
3D	three-dimensional
CT	Computed Tomography
DOE	Department of Energy
DWPF	Defense Waste Processing Facility
GFC	Glass Forming Chemical
HLW	High Level Waste
ICP-AES	Inductively Coupled Plasma – Atomic Emission Spectroscopy
JHCM	Joule-Heated Ceramic Melter
LAW	Low Activity Waste
LLNL	Lawrence Livermore National Laboratory
MRF	Melt Rate Furnace
NIST	National Institute of Standards and Technology
ORP	Office of River Protection
PNNL	Pacific Northwest National Laboratory
PUREX	Plutonium Uranium Extraction
REDOX	Reduction/Oxidation
SB	Sludge Batch
SMRF	Slurry-Fed Melt Rate Furnace
SRAT	Sludge Receipt and Adjustment Tank
SRNL	Savannah River National Laboratory
SRS	Savannah River Site
TTQAP	Task Technical and Quality Assurance Plan
WL	Waste Loading
WTP	Waste Treatment and Immobilization Plant

1.0 Introduction

The U.S. Department of Energy (DOE) is building the Waste Treatment and Immobilization Plant (WTP) at the Hanford Site in Washington to remediate 55 million gallons of radioactive waste that is being temporarily stored in 177 underground tanks. The low-activity waste (LAW) fraction will be partitioned from the high-level waste (HLW) during the feed pretreatment step and then each will be separately vitrified into borosilicate glass using Joule-heated ceramic melters (JHCM).[1]

Efforts are being made to increase the loading of Hanford tank wastes in glass while meeting melter lifetime expectancies as well as requirements for processing, regulatory compliance, and product quality.[2] The DOE Office of River Protection (DOE-ORP) has requested that the Savannah River National Laboratory (SRNL) support the advancement of glass formulations and process control strategies in various key technical areas, which include:

1. Nepheline crystallization in HLW glass
2. Development of crystal tolerant glasses
3. Enhanced HLW glass model applicability ranges
4. Corrosion evaluation of melter materials
5. Melting rate

Task 5 (melting rate) is the focus of this report. The experimental work was performed under an SRNL Task Technical and Quality Assurance Plan (TTQAP).[3] Tasks 1-4 were detailed in a separate TTQAP and will not be included in this report.[4]

1.1 Background

The overall mission life of WTP will be highly dependent on the waste loading (WL) of HLW and LAW in glass and on the glass production rate at each facility. Higher WL results in fewer glass canisters to be disposed of. Glass production rate is a function of (i) melting rate (time to convert incoming sludge-additive mixture to a glass product) and (ii) facility attainment defined as the percent of the time each facility produces waste glass at its design rate, including both scheduled and unscheduled outages. Ideally, increasing melting rate at the highest possible WL (or maximizing waste throughput) will shorten the overall mission life of Hanford waste cleanup.

Initial operations of the Defense Waste Processing Facility (DWPF) glass melter at the Savannah River Site (SRS) resulted in a correlation between WL and melting rate: as WL is increased, melting rate is decreased, which would ultimately lead to a longer mission life if maximum WLs were targeted. In order to balance between higher WL and higher melting rate, DWPF targeted a maximized waste throughput for the facility, which is defined as the maximum amount of waste being processed per unit time, as opposed to a maximum WL alone. Thus, maximizing waste throughput is a product of maximum WL and maximum melting rate. For DWPF, waste throughput was typically maximized at an intermediate WL range over which the specific sludge-frit compositions satisfy all process and product performance constraints.[5]

In order to improve glass production rates, both chemical and physical changes to the DWPF flowsheet have been focused on. Initial efforts for improved melting rate were chemical-based with the development and implementation of Frit 320 (replacing Frit 200) during processing of Sludge Batch 2 (SB2).[a] Given that SB2 was already prepared, adjustments to blending (i.e., alteration of the waste composition) or washing strategies (i.e., adjustment of the alkali concentration) could not be made so SRNL, partnering with the Pacific Northwest National Laboratory (PNNL), focused on developing an

[a] The primary difference between Frit 320 and Frit 200 was the total alkali content, 20 versus 16 wt% respectively.

alternative frit that would enhance melting rate.[6,7] The SRNL-PNNL efforts resulted in the implementation of Frit 320, which not only improved melting rate, but also allowed DWPF to increase WL from a nominal 28% to 34%. The dry-fed melt rate furnace (MRF) and its companion, the slurry fed-melt rate furnace (SMRF), played a critical role in isolating Frit 320 for SB2 implementation. This joint effort ultimately led to a significant shift in the DWPF strategy from a "one frit fits all" concept to the use of tailored frits for each sludge batch.

MRF testing at SRNL also suggested that melting rate is dependent on the source of alkali (sludge versus glass additives), especially in non-agitated melters.[8] More specifically, the results indicated that the extent that the SRS Tank Farm washed a sludge batch, which lowers the Na_2O concentration, must be balanced with the ability to add sufficient alkali to the frit to optimize melt rate. For example, during initial operations at DWPF, sludge batches were nominally washed to 0.5M Na^+ (similar to most WTP HLW feeds). Although these initial sludge batches processed through DWPF, it was not until the aforementioned joint SRNL-PNNL efforts to improve melting rate that the concept of a balanced alkali source was recognized. Although Frit 320 was developed and implemented for SB2 to improve melting rate, it served as the technical basis for a shift in washing strategy to balance the target washing endpoint with the ability to adjust the total alkali concentration in the frit to achieve maximum melting rates and optimize waste throughputs. Since SB3 DWPF has processed sludge batch washed to a nominal 1.0M Na^+ target.[b]

Although compositional changes (via tailored frits and different washing/blending strategies) were shown to be effective with respect to optimizing waste throughput for DWPF operations, physical changes were also developed and implemented to further improve melting rate. A lift pump was installed in the DWPF melter in 2004.[9] Glass was pumped from the bottom to the top of the melt pool, which resulted in a 5% gain in feed rate, 5% gain in melting rate and 10% gain in waste throughput. In 2010, the lift pump was replaced by four bubblers in the DWPF melter.[10] The instantaneous melting rate for the sludge batch being processed was increased from 59 kg/hr (130 lb/hr) to 91 kg/hr (200 lb/hr) during initial bubbler operation. Since bubbler implementation, no direct efforts have been made by the facility to increase WL to determine if waste throughput could be maximized at a higher WL range, while still satisfying process and performance constraints.

HLW glass melting is a complex process that involves a number of reactions and transformations that are initiated once feed enters the melter.[11] Most, if not all, of the complex reactions occur in the cold cap, which is defined as a porous solid crust of calcined slurry that floats on the surface of the glass melt.[12] The reaction pathways ultimately determine the amount of the time that is necessary to convert the melter feed slurry into a glass product (melting rate). Bubblers are effective in making more heat available to the batch material as it melts, thus improving contact between the batch and the molten glass; however, heat transfer, reactions among the batch components and gas evolution remain important factors that dictate melting rate, and ultimately waste throughput, regardless of forced convection. Key physical and chemical parameters that can influence melting rate include (but are not limited to):

- Compositional effects (feed chemistry – waste and glass additives)
- Form of the glass additives – frit versus glass forming chemicals (GFCs)
- Particle size of the GFCs or frit
- WL
- Forced convection (bubbling)
- Melter feed rheology
- Gas evolution and foaming

[b] It should be noted that the washing strategy must also consider other critical factors such as anion concentrations (e.g., S, F, Cl) and water management issues in the Tank Farm and evaporator systems.

- Reduction/Oxidation (REDOX) - source of reductants
- Formation of salts
- Physical properties of the cold cap and glass melt, such as specific heat, density, thermal diffusivity, and rate of heating

Therefore, identifying and understanding the impacts of feed chemistry and other process variables on melting rate remain important parts of the DOE waste immobilization mission and appropriate laboratory test methods must be developed to evaluate them.[13]

1.2 Melting Rate Measurement Technique

One of the primary screening tools being used at SRNL for relative melting rate comparisons is the MRF, in which a stainless steel beaker filled with dried, simulated melter feed is held at the desired melting temperature for a set amount of time. As previously mentioned, the results of the MRF have been used directly or in conjunction with SMRF testing to recommend frits and sludge preparation strategies to DWPF for sludge batches 1B through 6.[6,8,14-25] In addition, these tools have allowed WL versus melting rate curves to be generated, which have been used to demonstrate where optimal waste throughput can be achieved for a given melter feed.

Originally, the MRF beakers were cut in half after the melting test and the glass height was visually measured for each of the horizontal segments up to the red lines where relatively large-sized bubbles began to appear as shown in Figure 1-1.[14] The melting rate was determined as the average of all individual glass height readings divided by the time during which the sample was kept in the furnace at the target temperature. In 2006, digital radiography was used to view samples without having to physically cut the beakers in half.[20] X-ray images were collected in 0.5 degree increments over 360 degrees and then processed into a 3-dimensional (3D) volumetric data set using computed tomography (CT). The 3D data set was then sliced radially about the sample center, which produced an X-ray image that was similar in appearance to the beaker prepared for visual analysis (Figure 1-1). Although digital radiography eliminated the need to cut the beakers, melting rate was still determined by visual observations.

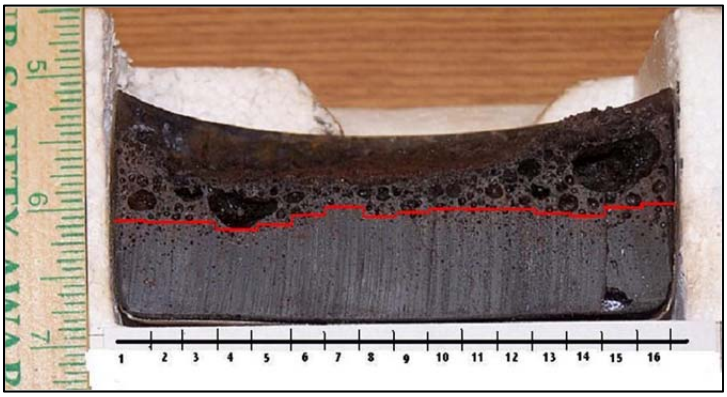

Figure 1-1. Determination of melting rates using the visual method.

One of the inherent technical difficulties with the visual melting rate measurement technique is determining the glass height in the presence of numerous gas bubbles of varying sizes. That is, the height at which the red lines in Figure 1-1 are drawn is subjective, which may influence the resulting melting rates significantly. For example, if the lines are drawn too low, a significant amount of glassy material interspersed among the gas bubbles will be excluded, thus underestimating melting rate. Likewise, if the lines are drawn too high, many large voids will be counted as glass and melting rate will be overestimated.

There is also no guarantee that a given distribution of the glass and gas bubbles along particular plane will always be representative of the entire sample volume. Although not perfect, the visual method has proved to be effective in identifying melting accelerants such as alkalis and sulfate that increased melting rate and allowed for ranking relative melting rates of candidate frits for a given DWPF waste chemistry. For example, the visual method was used to show that replacing Frit 418 with Frit 202[c] for the SB3 feed would result in a 10-30% decrease in melting rate, which was confirmed during the DWPF processing.[d,18]

In 2010, a new analysis approach was used for determining melting rate from the volumetric CT data set in order to eliminate much of the subjectivity associated with the visual melting rate measurement.[26] During X-ray scanning of the MRF beakers, some portion of the incident X-ray beam is absorbed by the sample and the remaining portion not absorbed is captured by a detector positioned on the other side. Radiographic attenuation is proportional to material density:

$$I = I_0 e^{-\mu L} \quad (1)$$

where I_0 and I are the intensities of the incident and attenuated X-ray beams, respectively, μ is the "material frequency" unique to each type of material in mm^{-1}, and L the material dimension or the size of the volume pixel, called voxel, in mm. Therefore, the exponent of Eq. (1) is dimensionless and the product of μ and L is specifically called the CT density. By definition, the CT density of a vacuum is zero because it contains no matter, so $I = I_0$. Voids of gas have a very small CT density so $I \approx I_0$. As the density of a material increases, the CT density also increases. The stainless steel beakers used in the MRF testing have a high enough CT density so $I << I_0$. Therefore, the product of a given CT density and the number of voxels of material having the same CT density will yield a relative measure of the total amount of material of that density. Since the CT density is dimensionless, the amount of material thus obtained is also dimensionless.

Each voxel of the material remaining in the beaker was categorized into one of the four zones in the order from the most to least dense as follows:

1. Melt: Fully melted glass with little or no gas bubbles.
2. Froth: Melted material interspersed among gas bubbles.
3. Un-melted: Feed material which may have begun to soften, but is still fundamentally in its original, loose granular form.
4. Below: Material of very low but non-zero density arising from voids of gas or the artifacts of radiography (x-ray beam-hardening, shadowing, etc.).

An example of a CT image and its corresponding colored image with zones 1-3 labeled is shown in Figure 1-2.

[c] Frit 418 ($8B_2O_3$-$8Na_2O$-$8Li_2O$-$76SiO_2$) and Frit 202 ($8B_2O_3$-$7Li_2O$-$2MgO$-$6Na_2O$-$77SiO_2$), in wt%.
[d] It should be noted that replacement of Frit 418 (the tailored frit for SB3) with Frit 202 was strictly an economical decision by DWPF. Due to an excess amount of the Frit 202 inventory, DWPF desired to consume it during SB3 processing in order to liberate storage space and minimize expenditures on procuring additional Frit 418. SRR requested that SRNL assess the impact of Frit 202 on melting rate and WL. Once the Frit 202 inventory was depleted, DWPF transitioned back to Frit 418.

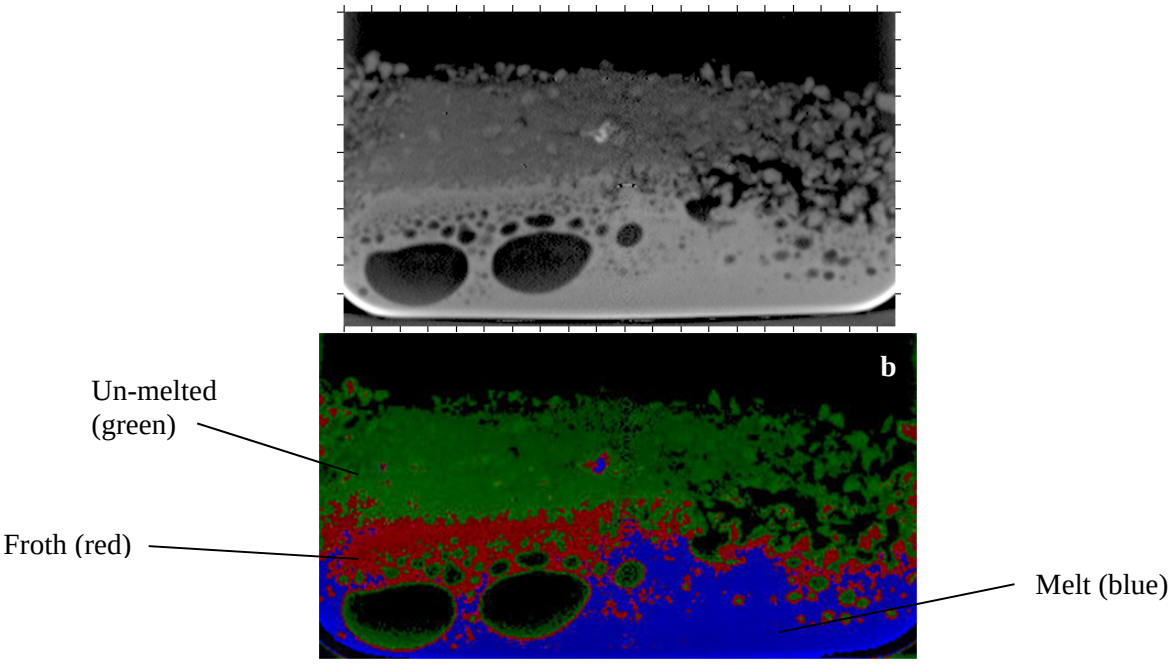

Figure 1-2. Example of a CT image (a) and corresponding colored image to differentiate the melt, froth and un-melt zones (b).

A histogram of CT density versus material amount of each zone was created from the 3D volumetric data as shown in Figure 1-3.[e] The threshold boundaries between two adjacent zones were determined by finding significant negative-to-positive zero crossings of the 3rd derivative of the histogram. This method was adopted in order to remove bias associated with determining the boundaries between material types. Generally, the zero-crossing points were at or near the midpoint between two adjacent histogram peaks produced by different material types. The integration of the resulting histogram over the CT density interval for a given zone gave the total amount of material present in that zone.

The melting rate rankings of the various 2010 samples were based on the total amount of material present in both the melt and froth zones as determined by the integration of the histogram peaks, which eliminated the subjectivity introduced by the visual measurement.[f] This new method of determining melting rates proved to be the most suitable compared to rankings based on the visual melting rate readings or material density. In the 2010 study, the melting rate rankings were also compared between the CT and visual methods. The accuracy of the visually determined melting rate was found to decrease with increases in the concentration of gas bubbles in the sample matrix.

[e] Material amount on the y-axis was calculated by multiplying a given CT density by the number of voxels having that CT density.
[f] From the standpoint of a continuously-fed melter operation, it seemed practical to include the froth material in the relative melting rate determination.

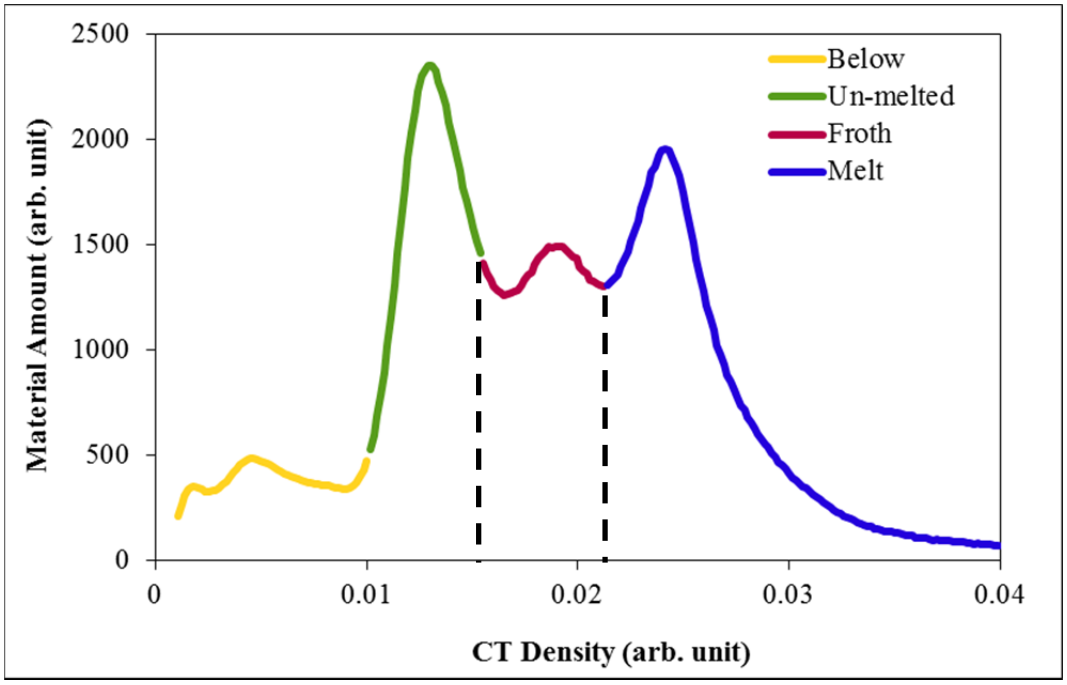

Figure 1-3. Example histogram of CT density versus material amount.

2.0 Objective

SRNL and PNNL are developing a joint melting rate program for DOE-ORP that is primarily focused on supporting the development of the melting rate model at PNNL, which could be used to support glass formulation strategies for WTP. As previously mentioned, there are numerous parameters that influence cold cap melting and it is important to identify laboratory test methods to discern the impact of these parameters on melting rate. Thus, the primary objectives of this preliminary melting rate task are as follows:

1. Assess the impact of frit and GFCs additives on the melting rate of two melter feed compositions
2. Compare the melting rate assessment techniques of SRNL (MRF/CT) and PNNL (pellet test) using the same melter feeds

The results of objective (1) will be the focus of this report. Once the results of the pellet tests conducted by PNNL have been documented in a separate report, objective (2) will be completed.

3.0 Experimental Procedure

3.1 Melter Feed Selection

Two sets of MRF run feeds were fabricated for this task with simulated SB6 Sludge Receipt and Adjustment Tank (SRAT) product using glycolic acid as the reductant.[g,27] This SRAT product was selected as there was a sufficient quantity already on hand that would satisfy the needs for this task, thus avoiding programmatic delays to perform these initial melting rate tests. In addition, the SRAT product selected was based on an alternative reductant flowsheet being considered for DWPF (i.e., replacing

[g] In DWPF, the waste slurry received from the Tank Farms undergoes pretreatment processes in the SRAT before being blended with frit and fed to the melter. The SB6 simulant used for these melting tests went through an abbreviated SRAT cycle at Harrell Industries, Inc. in 2013.

formic acid with glycolic acid as the baseline reductant).[h] The analytical results of the SB6 SRAT product are shown in Table 3-1.[28] This nitric-glycolic acid SRAT product composition was characterized by more than three times higher nitrate level per mole of carbon than the nitric-formic acid baseline[29] and a target Na^+ molarity of approximately 1.4M.

The glass additive compositions and WLs were defined by the PNNL 2009 and 2013 glass algorithms using the composition of the DWPF SB6 SRAT product.[2,30] Target compositions of the melter feeds are shown in Table 3-2. For simplification, the melter feeds based on the 2009 and 2013 algorithms will be referred to as "high boron" and "low boron" melter feeds, respectively, for the remainder of this report. The components in bold (B_2O_3, Li_2O and Na_2O) highlight the main differences between the two compositions. These feed compositions were derived using different WLs; 35.09% for the high boron feed and 39.22% for the low boron melter feed.

Table 3-1. Analytical Results of SB6 SRAT Product Based on Glycolic-Acid Addition

Element	wt% calcined	Anion	mg/kg
Al	13.5	F	<500
Ba	0.133	Cl	417
Ca	1.12	NO_2	<500
Cr	0.175	NO_3	67,000
Cu	0.125	$C_2H_3O_3$	44,500
Fe	21.3	SO_4	1,860
K	0.313	C_2O_4	2,010
Mg	0.852	HCO_2	3,140
Mn	6.83	PO_4	<500
Na	13.8	**Solids**	**wt%**
Ni	2.95	Total	32.3
P	<0.100	Insoluble/Soluble	15.8/16.5
S	0.354	Calcine	18.0
Si	1.42	**Density**	**g/mL at 25°C**
Sn	0.06	Slurry	1.25
Ti	0.051	**pH**	5.03
Zn	0.111		
Zr	<0.100		

[h] MRF testing has not previously been conducted at SRNL using the alternate reductant nitric-glycolic flowsheet melter feed. Therefore, the protocols to be applied in the preliminary DOE-ORP testing will be based on the run conditions proven effective for the baseline nitric-formic acid flowsheet.

Table 3-2. Target Melter Feed Compositions (wt%)

Component	2009 Algorithm (High Boron)		2013 Algorithm (Low Boron)	
	Additive	***Melter Feed***	***Additive***	***Melter Feed***
	35.09% Waste Loading		**39.22% Waste Loading**	
Al_2O_3	---	8.95	---	10.00
B_2O_3	**30.81**	**20.00**	**14.18**	**8.62**
BaO	---	0.05	---	0.06
CaO	---	0.55	---	0.61
Cr_2O_3	---	0.09	---	0.10
CuO	---	0.05	---	0.06
Fe_2O_3	---	10.69	---	11.94
K_2O	---	0.13	---	0.15
Li_2O	**0.48**	**0.31**	---	**0.00**
MgO	---	0.50	---	0.55
MnO	---	3.09	---	3.46
Na_2O	**11.25**	**13.83**	**25.25**	**22.64**
NiO	---	1.32	---	1.47
P_2O_5	---	<0.08	---	<0.09
SO_3	---	0.31	---	0.35
SiO_2	57.46	38.36	60.57	38.01
SnO_2	---	0.03	---	0.03
TiO_2	---	0.03	---	0.03
ZnO	---	0.05	---	0.05
ZrO_2	---	<0.05	---	<0.05

3.2 Frit Fabrication

Raw materials were selected from the current list of baseline GFCs that were characterized in WSRC-TR-2002-00282.[31] Details for the specific GFCs used in this task are shown in Table 3-3.

Table 3-3. Glass Forming Chemicals

Oxide	Mineral	Grade	Vendor
B_2O_3	Boric Acid – H_3BO_3	Technical Grade - Granular	U.S. Borax
Na_2O	Na_2CO_3 Anhydrous	Dense Soda Ash	Solvay Minerals
Li_2O	Li_2CO_3	Technical Grade	Chemettal-Foote
SiO_2	SiO_2	SCS-75	U.S. Silica

Each frit was prepared from the proper proportions of the GFCs in 500 g batches.[32] The raw materials were thoroughly mixed and placed into uniquely identified platinum alloy crucibles. Each crucible was placed into a high-temperature furnace at 1100°C for 30 minutes with a loose-fitting lid.[33] At the end of the isothermal hold, the crucibles were removed and the molten glass was poured onto a clean, stainless steel plate and allowed to air cool. Un-melted material was observed in the high boron glass, so the pour

patty was broken up into pieces and re-melted at 1150°C for 30 minutes. The resulting glass from both compositions was ground and sieved to -80/+200 mesh (74-177 µm) targeting the particle size specifications for DWPF.[34] Frits were stored until use in marked containers using unique identifiers.

3.3 Melter Feed Fabrication

Prior to use, the SRAT product was homogenized using a stand mixer. Once mixed, the SRAT product was blended with either GFCs or frit to yield 50 grams (SRNL MRF testing) or 30 grams (PNNL pellet testing) of glass according to a mass ratio determined by the target WL and the measured calcination ratio of the SRAT product. The melter feeds were thoroughly mixed and poured into uniquely labeled stainless steel pans. Blended feed was dried in an oven at ~100 °C overnight and the dried melter feed was passed through a 10-mesh (1.7 mm) screen. This method is consistent with the preparation of melter feeds to support previous baseline nitric-formic acid flowsheet MRF testing. Screened materials were stored until use in marked containers using unique identifiers.

3.4 Compositional Analysis

To confirm that the as-fabricated frits corresponded to the defined target compositions of the high and low boron additives, a representative sample of each glass was submitted for chemical analysis. Two dissolutions techniques were utilized: sodium peroxide fusion and lithium metaborate fusion.[35,36] Each frit was prepared in duplicate for each dissolution technique and analyzed by Inductively Coupled Plasma – Atomic Emission Spectroscopy (ICP-AES). The instrument was calibrated prior to analyzing the samples and check standards were analyzed before and after the samples per procedure to verify the performance of the ICP-AES over the course of the analyses.[37]

Representative melter feed samples fabricated from both frit and GFCs were also submitted for analysis. Two dissolutions techniques were utilized: sodium peroxide fusion and lithium tetraborate fusion.[35,38] These samples were measured by ICP-AES using the method described in the previous paragraph.

Once the melter feed compositions were confirmed to be consistent with the target compositions, samples were shipped to PNNL to support the pellet tests.

3.5 Glass Density

Prepared melter feed samples were placed into uniquely identified platinum alloy crucibles. Each crucible was placed into a high-temperature furnace at 1150°C for 1 hour with a loose-fitting lid.[33] At the end of the isothermal hold, the crucibles were removed and the molten glass was poured onto a clean, stainless steel plate and allowed to air cool. The pour patty was broken and samples were selected for the density measurement.

The density of representative samples of each of the as-fabricated glasses was measured in duplicate via the Archimedes method.[39] A National Institute of Standards and Technology (NIST) glass density standard 1826 was measured prior to each set of samples as an internal check of the measurement technique.

3.6 MRF Operation

In preparation for MRF testing, melter feed was placed into a uniquely identified, 54 mm diameter and 67 mm high stainless steel beaker. The beaker was wrapped with a single layer of 3 mm thick insulating felt. The wrapped beaker was placed into an insulating sleeve and covered with a vented insulation board. The insulating felt is used to fill the gap between the beaker and the interior side wall of the sleeve and minimizes any side heating that could occur in the furnace during melting rate testing. This configuration is desired in order to impose a vertical temperature profile within the beaker that is similar to the one-dimensional heating from the melt pool that the feed experiences in the cold cap of an actual melter.

The MRF is a top loading crucible furnace with a cylindrical inner chamber that is 222 mm in diameter. The bottom 229 mm of the chamber is heated by helical wire coils that are embedded in the insulation. A schematic of the furnace is shown in Figure 3-1. Once the furnace setpoint reaches 1150°C, the cover is removed and the insulating sleeve containing the beaker is lowered into the furnace. When inserted, the bottom of the beaker was recessed by approximately 38 mm from the bottom of the insulating sleeve, which was flush with the top of the uppermost heating coil. After twenty minutes, the insulated beaker assembly was removed from the furnace and allowed to cool in air. This firing duration was found to be long enough to melt some of the melter feed, but still short enough to leave a portion of the feed partially melted or completely un-melted. The furnace temperature was monitored during each firing to ensure that the conditions were similar for each sample. It was necessary to have a twenty minute wait period between successive tests so that the furnace returned to a stable temperature.

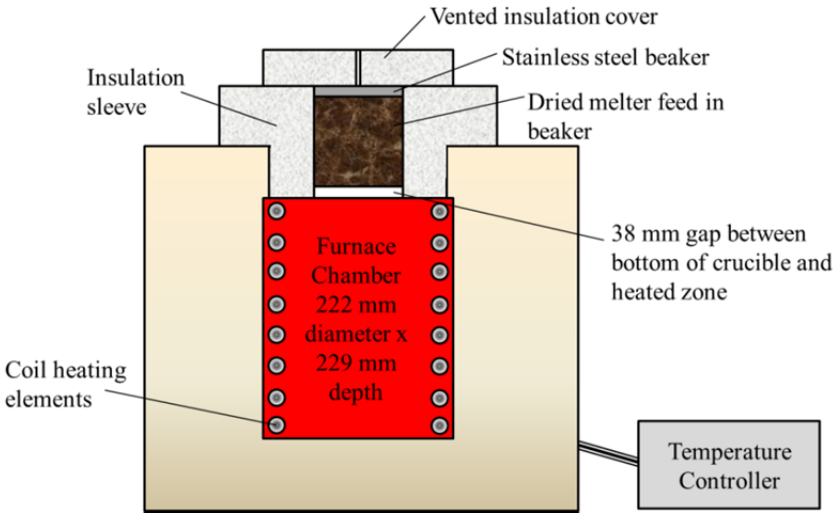

Figure 3-1. Schematic of the MRF (not to scale).

3.7 X-Ray Computed Tomography

Once beakers were removed from the furnace after each firing, they were cooled in ambient air. The cooled beakers containing both melted glass and loose feed material were analyzed by X-ray CT scan. X-ray images of the beaker contents were taken using an SRNL developed lens-coupled digital radiography system consisting of a GE/Seifert 420 Isovolt X-ray generator, an IQI high density doped glass scintillation screen and a Roper Scientific, Quantix CCD camera fitted with a Nikon Nikkor 85 mm lens. A four-axis motion control system from New England Affiliated Technologies was used for sample positioning. Control and processing software was written in-house, using National Instruments LabVIEW programming language. For each sample, 360 digital radiographs were taken at an angular increment of 1 degree. The potential at the X-ray source was set at 300 KV. 2.3 mm iron and 1.0 mm copper were used at the X-ray source to harden the source beam and a 0.13 mm lead filter was used at the scintillator to attenuate X-ray scatter. Feldkamp cone-beam reconstruction was performed on the sample data using Imgrec software developed at Lawrence Livermore National Laboratory (LLNL) to produce a 3D volumetric data set at a resolution of 0.0014 mm^3 voxel.

A post reconstruction image processing algorithm was applied to each CT slice, which mathematically removed the stainless steel beaker wall and its artifacts. This algorithm first constructed a radial intensity profile of the beaker and interior from the reconstruction slices above the material (containing only the beaker) and then subtracted this profile from the CT slices in the entire dataset. By removing the beaker and its associated X-ray artifacts the material adhering to the beaker wall could be included in the analysis.

3.8 Quality Assurance

Requirements for performing reviews of technical reports and the extent of review are established in manual E7 2.60. SRNL documents the extent and type of review using the SRNL Technical Report Design Checklist contained in WSRC-IM-2002-00011, Rev. 2.

4.0 Results and Discussion

4.1 Frit Fabrication

A comparison of the target versus measured compositions of the fabricated frits is shown in Table 4-1.

Table 4-1. Comparison of Target and Measured Frit Compositions

	High Boron		Low Boron	
	Target (wt%)	Measured (wt%)	Target (wt%)	Measured (wt%)
B_2O_3	30.81	28.83	14.18	13.61
Li_2O	0.48	0.44	---	ND
Na_2O	11.25	11.26	25.25	25.52
SiO_2	57.46	58.47	60.57	61.97

ND – Not detected

In general, the measured concentrations were consistent with the targets; however, the B_2O_3 content for the high boron frit was 2 wt% lower than the target. The sample was re-analyzed, but the results were similar. Thus, it was hypothesized that some of the boron added as H_3BO_3 volatilized during melting even though a loose-fitting lid was used. In order to account for potential volatility, the frit components were re-batched with an excess of 2.5 wt% B_2O_3 above the target. The resulting frit composition had a B_2O_3 content that was more representative of the target as shown in Table 4-2.

Table 4-2. Target and Measured Compositions for the Re-batched Frit

	High Boron Additive Re-batched		
	Target (wt%)	Measured (wt%)	% Difference
B_2O_3	30.81	30.41	-1
Li_2O	0.48	0.50	4
Na_2O	11.25	10.60	-6
SiO_2	57.46	57.04	-1

4.2 Melter Feed Fabrication

A comparison of the target versus measured compositions of the melter feeds is shown in Table 4-3 on an oxide basis. It should be noted that the high boron melter feed was measured with the original frit (prior to the re-batching), thus the boron content is low. Since the re-measured frit composition (Table 4-2) was consistent with the target, the composition of the re-batched melter feed was not re-measured. Besides the deviation of the boron content in the high boron melter feed made with frit, all other major components (> 0.5 wt%) are relatively consistent with the target concentrations. To be clear, the MRF and pellet tests will be based on the use of melter feeds with the re-batched high boron content frit.

Table 4-3. Target and Measured Melter Feed Compositions (wt%)

Oxide	High Boron					Low Boron				
	Target	Measured Frit	% Difference	Measured GFCs	% Difference	Target	Measured Frit	% Difference	Measured GFCs	% Difference
Al_2O_3	8.95	9.33	4	9.12	2	10.00	10.38	4	9.91	-1
B_2O_3	20.00	17.45	-13	19.22	-4	8.62	7.59	-12	8.35	-3
BaO	0.05	0.06	7	0.05	4	0.06	0.06	8	0.06	4
CaO	0.55	0.55	0	0.52	5	0.61	0.61	1	0.58	-5
Cr_2O_3	0.09	0.10	13	0.09	6	0.10	0.12	19	0.11	6
Fe_2O_3	10.69	11.26	5	10.88	2	11.94	12.50	5	12.02	1
K_2O	0.13	0.14	9	0.14	4	0.15	0.15	3	0.15	0
Li_2O	0.31	0.43	38	0.40	30	0.00	<0.22	---	<0.22	---
MgO	0.50	0.53	8	0.51	3	0.55	0.60	8	0.58	4
MnO	3.09	3.40	10	3.24	5	3.46	3.73	8	3.59	4
Na_2O	13.83	13.14	-5	13.23	-4	22.64	21.69	-4	22.24	-2
NiO	1.32	1.44	9	1.39	5	1.47	1.57	6	1.53	4
P_2O_5	<0.08	<0.23	---	<0.23	---	<0.09	<0.23	---	<0.23	---
SO_3	0.31	0.25	-19	0.23	-27	0.35	0.38	10	0.35	0
SiO_2	38.36	39.43	3	39.71	3	38.01	37.38	-2	38.28	1
SnO_2	0.03	<0.13	---	<0.13	---	0.03	<0.13	---	<0.13	---
TiO_2	0.03	<0.17	---	<0.17	---	0.03	<0.17	---	<0.17	---
ZnO	0.05	<0.12	---	<0.12	---	0.05	<0.12	---	<0.12	---
ZrO_2	<0.05	0.13	---	0.13	---	<0.05	0.15	---	0.15	---

4.3 X-ray CT Images

The X-ray CT images of the beakers after the heat treatment are shown in Figure 4-1. These images were taken along the cross-section through the center axis perpendicular to the X-ray source. Each sample consists of four distinctive morphological zones. First, the large void in the middle of each image was created mainly by the generation of calcine gases. In a previous study, voids of varying sizes were still observed in frit-only samples that contained no gas generators, so it is also speculated that pockets of air present in the fresh feed also contribute to void formation, though to a lesser degree than calcine gas formation.[26] The bottom zone below the large void in each of the images in Figure 4-1 represents fully-melted glass relatively free of large gas bubbles, while the top zone contains not-yet-melted material in or near its original form. Lastly, the middle zone between the top zone and the large void in the middle contains more potentially melted material interspersed among numerous bubbles of differing sizes.

Visually, it appears that the glass level height for the high boron feed is comparable for both frit and GFCs; however, the glass resulting from melter feed made with the GFCs does contain a number of large bubbles. Bubbles are also present in the GFCs-based low boron feed sample and it appears that the glass height of the frit-based melter feed sample is slightly higher and nearly free of bubbles. Although the X-ray CT images allow a visual assessment of the interior of the sample, it is recognized that this view is not representative of the entire sample and thus this information is not used to make any conclusions with respect to the objectives of this preliminary test series. The subsequent analysis and discussion of the sample results will take into account the entire 3D data set as opposed to a two-dimensional (2D) image of a particular cross-section.

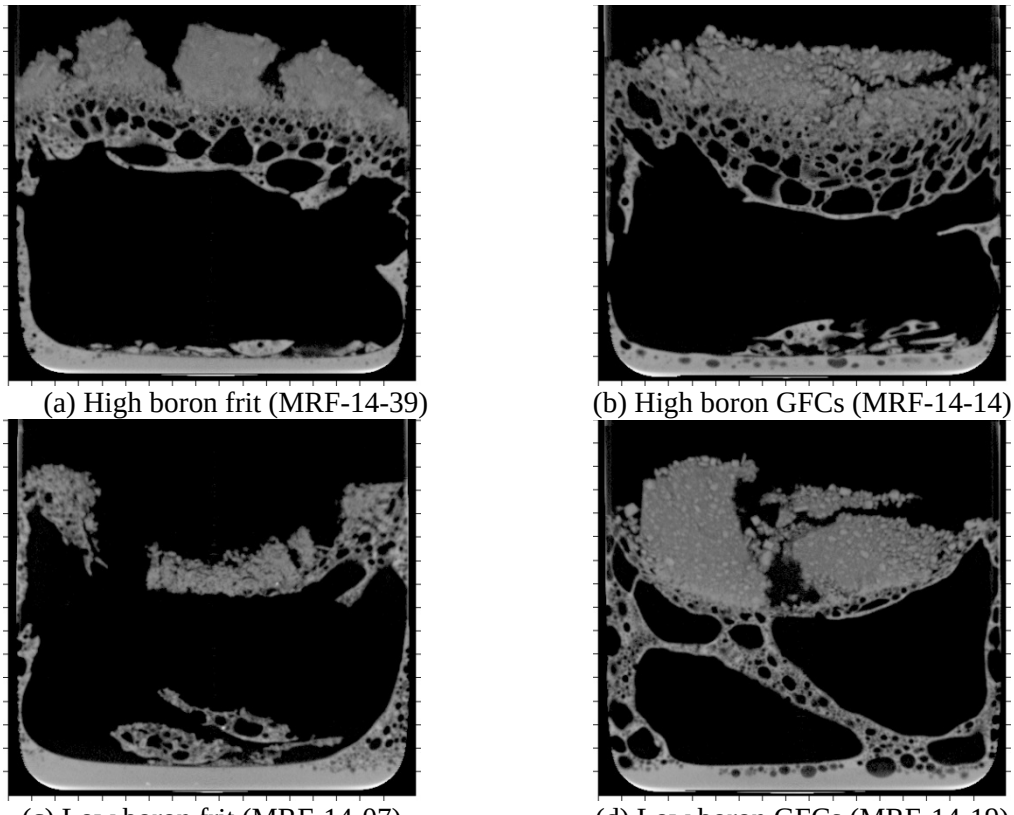

(a) High boron frit (MRF-14-39) (b) High boron GFCs (MRF-14-14)

(c) Low boron frit (MRF-14-07) (d) Low boron GFCs (MRF-14-19)

Figure 4-1. X-ray CT images of the high and low boron melter feeds after firing.

CT histogram pictures, called histopics, are shown in Figure 4-2 and are paired with X-ray images for comparison. Each histopic represents a vertical profile of material or CT density count; the y-axis

represents the elevation within the beaker, while the x-axis represents the CT density. It should be noted that the histopics present 3D information as each one is a composite of all 360 images taken for each sample. As more material is found at a given CT density, the color changes from blue (lowest count) to green, yellow and finally to red (highest count). For example, all histopics except for the low boron frit feed show large patches of green at the same elevation as the un-melted feed material and their x-coordinates are in the lower end of the CT spectrum, confirming that they consist mostly of un-melted feed material. The very faint green patch of the low boron frit feed is in agreement with its X-ray image that shows a much lower quantity of un-melted material remaining compared to the other samples. As expected, the patches of green shift to the right (higher CT density) at low elevation, since the material compacts as it melts. Both the high and low boron feeds fabricated using frit also contain small, faint yellow areas at low elevation and high CT density, which suggests that these two samples formed the most glass during firing. The red patches along the left edge of each histopic signify the presence of a high concentration of very low CT density material or voids throughout much of the vertical dimension of the beaker except where melted and un-melted materials are located, as observed in the X-ray images.

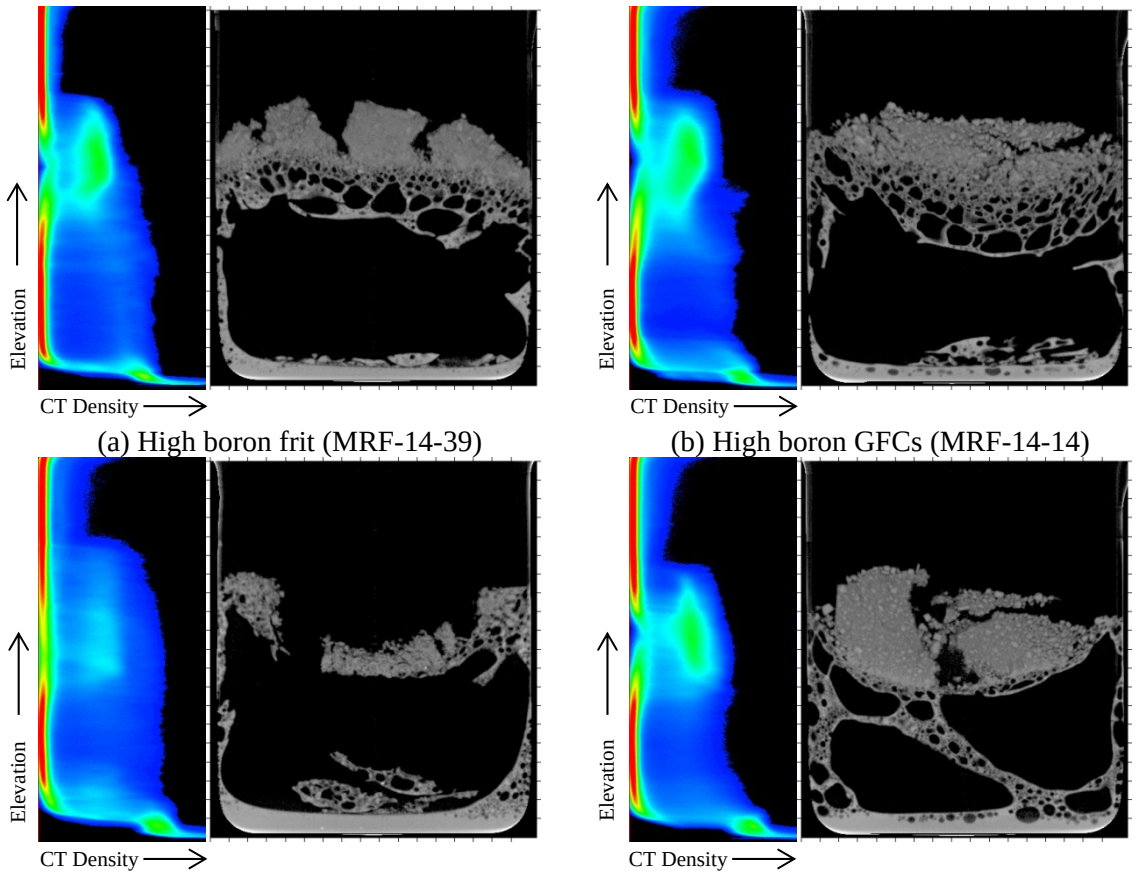

(a) High boron frit (MRF-14-39) (b) High boron GFCs (MRF-14-14)

(c) Low boron frit (MRF-14-07) (d) Low boron GFCs (MRF-14-19)

Figure 4-2. Comparison of the CT histopics and CT images for the high and low boron melter feeds.

4.4 CT Analysis Results

Histograms of CT density versus material amount for the 3D data set of each sample are shown in Figure 4-3 and Figure 4-4. Unlike the example provided in Figure 1-3 containing three peaks which were named as melted, froth and un-melted zones, the feeds used in this study produced only two distinct peaks and they were assigned as melted and un-melted zones since the lower of the two peaks in each histopic was comparable to the CT density of the un-melted zone in Figure 1-3.[26] It is possible that the froth material

is present; however, the CT density of the froth zone could not be distinguished from the un-melted zone in these particular samples.

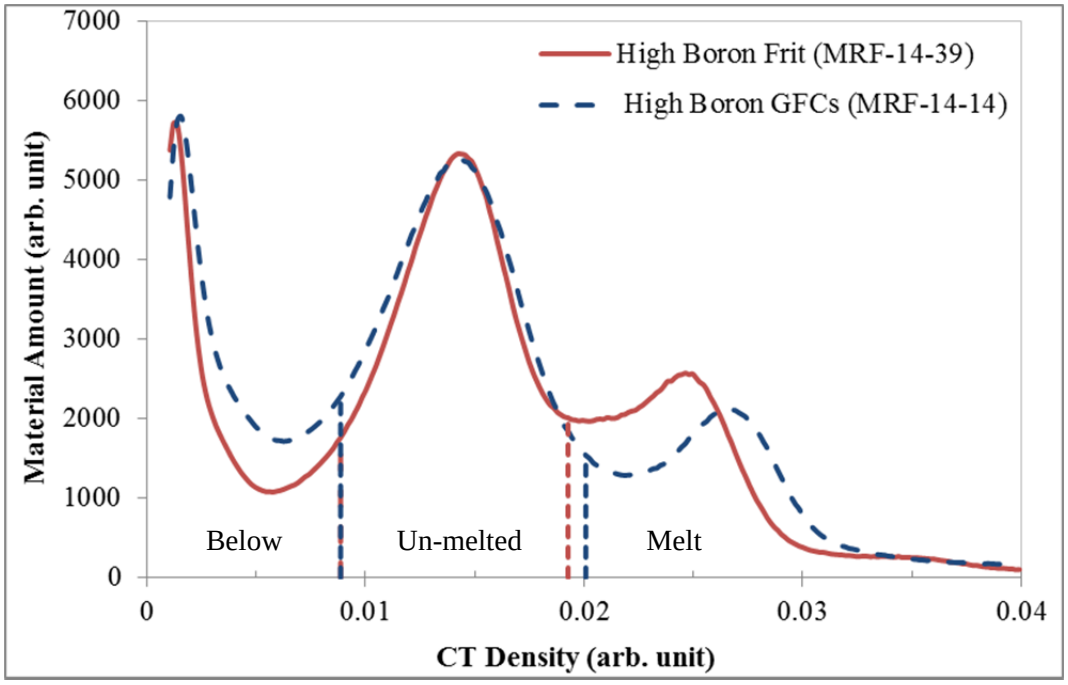

Figure 4-3. Comparison of the histograms for the high boron melter feed.

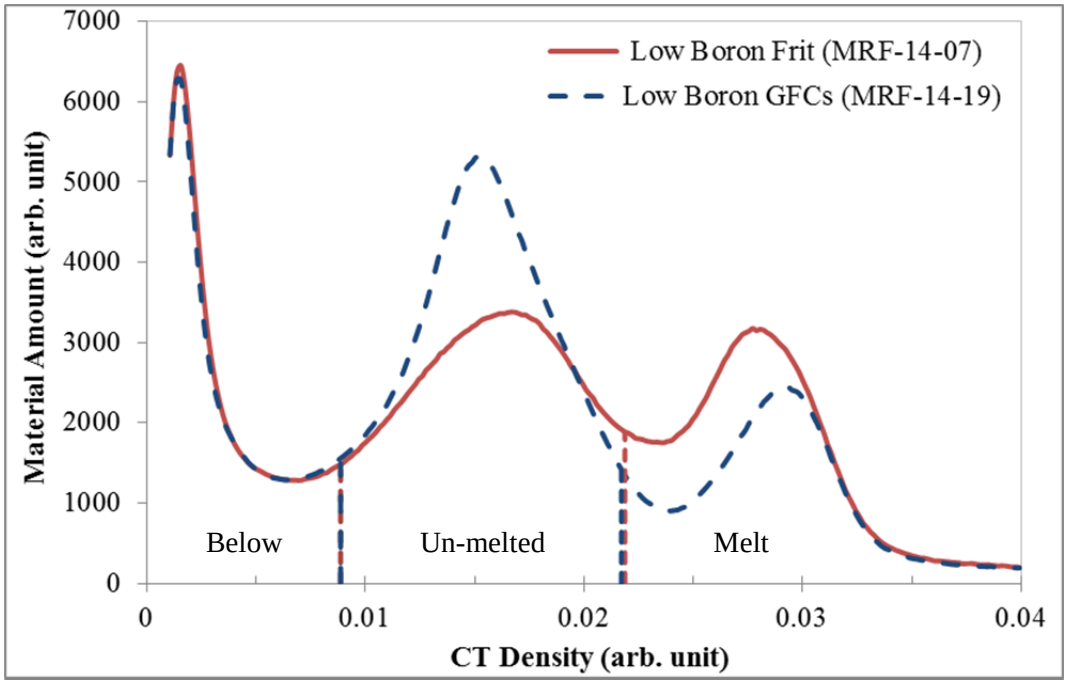

Figure 4-4. Comparison of the histograms for the low boron melter feed.

Generally, the transition point between the un-melted and melt zones was consistent and remained in the CT density range of 0.019-0.022, which is comparable to the previous study.[26] The CT density at which un-melted material was differentiated from very low density material was 0.009 for all samples. The

simulated SRAT product used in this study was prepared using a new flowsheet based on nitric and glycolic acids and, as a result, contained a considerably higher concentration of gas generators[i] than feeds used in previous studies based on the DWPF baseline nitric-formic acid flowsheet. The presence of excess gas generators in the nitric-glycolic acid melter feed likely contributed to a greater expansion of the melter feed and thus potentially a lower melting rate. The impact of acid addition (formic versus glycolic acid) on melting rate will be discussed in a subsequent report.

In order to determine the quantitative relative melting rates, the amount of material in each of the un-melted and melted zones was calculated by determining the area under their respective CT histogram peaks.[j] The results are tabulated in Table 4-4.

Table 4-4. CT-Calculated Distribution of Material

Sample ID	Additive Form	Material Amount		
		Total	Un-melted	Melt
High Boron (35.09% WL)				
MRF-14-39	Frit	360,544	229,891	130,652
MRF-14-14	GFCs	362,324	252,871	109,453
% Difference	---	0	10	18
Low Boron (39.22% WL)				
MRF-14-07	Frit	368,171	209,713	158,459
MRF-14-19	GFCs	372,583	259,162	113,422
% Difference	---	1	21	33

Since each beaker was filled with enough melter feed to form 50 grams of glass, the total amount of material should be fairly constant for samples prepared at the same WL. As shown in Table 4-4 there was no measureable difference in the total amount of material for the high boron melter feed samples and approximately 1% difference in the low boron melter feed samples. The low variation of the total sample amount within a sample set demonstrates that there is consistency with this CT analysis technique.

Among the four samples, the low boron frit melter feed had both the highest amount of melted material and least amount of un-melted material. In both feed compositions, the frit melter feeds produced more melted material than the GFCs-based melter feeds; however, the percent difference between frit and GFCs was larger for the low boron than the high boron melter feed (approximately 33% versus 18%).

Regardless of whether the SB6 SRAT product was blended with frit or GFCs, the low boron melter feeds resulted in more melted material than the high boron melter feed counterparts despite the higher WL of the low boron melter feed. Previous studies with the DWPF baseline nitric-formic acid flowsheet have shown that melting rate decreases with increasing WL for a particular waste composition.[5,26] Since the low boron melter feeds contained ~64% higher total sodium than the high boron melter feeds, it is likely that the excess sodium was more than enough to overcome the negative impact of the higher WL. Since no other MRF studies have been performed with the nitric-glycolic acid flowsheet, it is not certain whether the inverse relationship between melting rate and WL observed with the nitric-formic acid flowsheet melter feeds would be still applicable to the melter feed used in this study. The WL versus melting rate trend for the nitric-glycolic acid flowsheet melter feed will be compared to the nitric-formic acid flowsheet melter feed in a subsequent report.

[i] Gas generators were mainly in the form of nitrated salts.
[j] The product of a given CT density and the number of voxels of material having the same CT density will yield a relative measure of the total amount of material of that density.

For ease of comparison, the material amounts tabulated in Table 4-4 were plotted in Figure 4-5 along with 10% error bars in order to demonstrate the potential variation present in this analysis technique.[k] There is some overlap of the error bars for the high boron melter feeds, which suggests that there are minimal or no significant differences in melting rate between the frit and GFCs based on the limited results of this study. It is possible that more of a difference between melting rate could be discerned in the future once the variation amongst samples can be better quantified. Conversely, there is no overlap of the error bars for the low boron feeds, which indicates that frit-based melter feed has a faster melting rate than GFCs-based melter feed. In summary, the relative melting rate rankings are as follows:

- High boron melter feed – Minimal or no difference in melting rate between frit and GFCs
- Low boron melter feed – Faster melting rate can be achieved with frit rather than GFCs

Due to the difference in WL for the high and low boron melter feeds (35.09% versus 39.22%, respectively), a relative melt rate ranking amongst all four samples will not be presented.

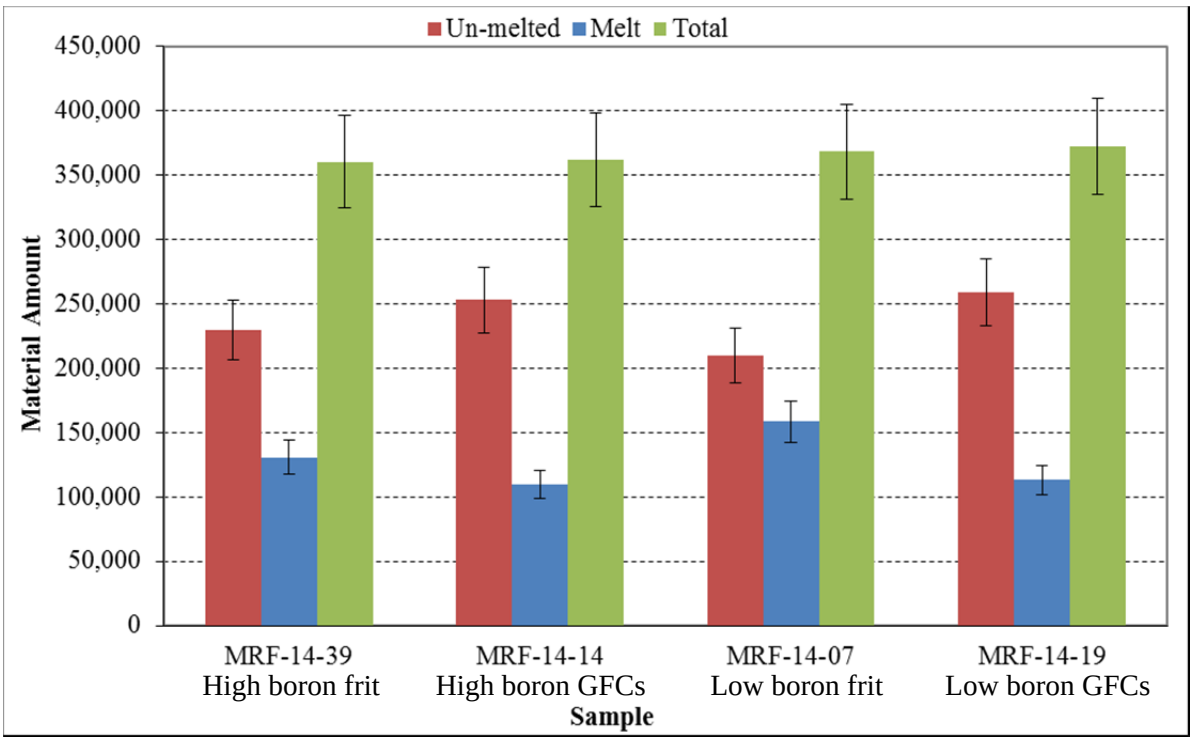

Figure 4-5. Comparison of material amounts for the high and low boron melter feeds.

4.5 Effect of Gas Generators on Melting Rate

A previous study based on the DWPF nitric-formic acid baseline flowsheet demonstrated that melting rate of a given feed decreases with increases in the concentration of gas generators such as $NaNO_3$.[26] While the addition of frit does not increase the concentration of gas generators, the addition of GFCs produces both H_2O and CO_2 from the decomposition of boric acid and sodium/lithium carbonate, respectively, and thus could have a negative impact on melting rate. The waste feed and glass additives undergo complex physical and chemical transformations as they decompose, calcine and melt before being fused into glass, and it is during the decomposition/calcination stages when much of the gases are released. In this work, the gas evolution through each stage of melting of the waste/frit and waste/GFCs feeds was estimated at 100% conversion. The concept of staged melting comes from the DWPF cold cap model, which

[k] A limited scoping test on repeatability suggests that 10% may be bounding; however, there will be more of an opportunity to further quantify variation in future test sets.

approximates melting of the feed solids as a continuous, 4-stage countercurrent process with the temperature of each stage set progressively higher from the top (Stage 1) to bottom (Stage 4).[40] The DWPF model assumes that non-volatile feed components decompose and calcine as they move down each stage, releasing gases as follows:

Stage 1:	$2\ Fe(OH)_3 \rightarrow Fe_2O_3 + 3\ H_2O\ (g)$	(1)
	$2\ B(OH)_3 \rightarrow B_2O_3 + 3H_2O\ (g)$	(2)
	$2\ NaCOOH \rightarrow Na_2C_2O_4 + H_2\ (g)$	(3)
	$Na_2C_2O_4 \rightarrow Na_2CO_3 + CO\ (g)$	(4)
	$2\ NaNO_3 \rightarrow 2\ NaNO_2 + O_2\ (g)$	(5)
	$2\ NaNO_2 \rightarrow Na_2O + NO\ (g) + NO_2\ (g)\ (30\%)$	(6)
Stage 2:	$2\ NaNO_2 \rightarrow Na_2O + NO\ (g) + NO_2\ (g)\ (50\%)$	(6)
	$Na_2CO_3 \rightarrow Na_2O + CO_2\ (g)$	(7)
	$Li_2CO_3 \rightarrow Li_2O + CO_2\ (g)$	(8)
Stage 3:	$2\ NaNO_2 \rightarrow Na_2O + NO\ (g) + NO_2\ (g)\ (20\%)$	(6)
	$Fe_2O_3 \leftrightarrow 2\ FeO + ½\ O_2\ (g)$	(9)
	$3\ Fe_2O_3 \leftrightarrow 2\ Fe_3O_4 + ½\ O_2\ (g)$	(10)

Note that decomposition of nitrate/nitrite is allowed to continue into Stage 3. Eqs. (9) and (10) represent redox-equilibrium reactions and do not contribute significantly to the overall gas production. The resulting molar evolution of calcine gases from the high boron GFCs-based feed (MRF-14-14) is shown in Table 4-5 as an example per 50 g of glass produced. Gases produced in Stages 1 and 2 account for ~95% of the total gas evolution and ~50% of the gases produced in Stage 1 come from the decomposition of $B(OH)_3$, one of the four GFCs. Including Stage 2, the addition of GFCs increases the overall gas evolution by ~67% over that of the high boron frit-based feed (MRF-14-39).

Table 4-6 summarizes the maximum gas evolution for the DWPF melter feeds during each stage of calcination/melting of a batch containing enough feed to produce 50 g of glass at 100% melting. The gas evolution from Stage 3 is the same regardless of frit or GFCs, since the decomposition of GFCs is complete by Stage 2. Furthermore, gas evolution continues in Stage 4, but is not shown since gas evolution is mostly due to redox-equilibrium reactions, which produces even less gas than Stage 3.

Table 4-5. Maximum Gas Evolutions from High Boron GFCs-Based Melter Feed (per 50 g glass)

Gases	Stage 1 (gmole)	Stage 2 (gmole)	Stage 3 (gmole)
H_2O	0.73	0.04	0.02
CO_2	0.06	0.13	0.02
O_2	0.02	0.03	0.01
NO	0.04	0.04	0.02
NO_2	0.03	0.02	0.01
HCOOH	0.001	0	0
CH_4	0.01	0	0
Total	0.88	0.27	0.08
Contribution from GFCs			
H_2O	0.43	0	0
CO_2	0	0.06	0

Table 4-6. Maximum Gas Evolution from Dried MRF Batch (per 50 g Glass)

Sample ID	Additive	Stage 1	Stage 2	Stage 3	Total	H_2O+CO_2 from GFCs	CO_2 from GFCs
		(gmole)	(gmole)	(gmole)	(gmole)	(% total)	(% total)
High Boron (35.09% WL)							
MRF-14-39	Frit	0.45	0.21	0.08	0.74	0	0
MRF-14-14	GFCs	0.88	0.27	0.08	1.23	40	5
Low Boron (39.22% WL)							
MRF-14-07	Frit	0.50	0.23	0.09	0.82	0	0
MRF-14-19	GFCs	0.68	0.36	0.09	1.13	27	11

Higher gas evolution in Stage 1 from each GFCs-based feed as compared to its frit-based counterpart is due to H_2O vapor produced from the decomposition of boric acid (H_3BO_3), while higher gas evolution in Stage 2 from each GFCs-based feed is due to CO_2 from the decomposition of carbonates at higher temperatures. Table 4-6 also shows that the total gas evolution from the GFCs-based feeds is 40% and 27% higher than that from the frit-based counterparts containing high and low boron, respectively. In a previous MRF study, it was shown that increases in gas evolution cause a greater batch expansion, which leads to a reduction in heat transfer to the upper regions of the batch and thus typically lowers melting rates.[26] Thus, based on the excess gas evolution (H_2O and CO_2), one would expect the melting rates of high boron feeds to be impacted more by the use of GFCs than the low boron feeds, which is contrary to the CT results in Table 4-4; it is the low boron feed whose melting rate was impacted more by the use of GFCs rather than frit (18% (high boron) versus 33% (low boron) difference between frit and GFCs). If only the evolution of CO_2 is considered, then the CT-based melting rate trend can be predicted; the evolution of excess CO_2 from the GFCs increases the total gas evolution from the high and low boron feeds by 5% and 11% above those from the frit-based counterparts, respectively. These results appear to be consistent with the assumption made in the previous study; gases evolving in the early stages of melting such as H_2O vapor have a better chance of venting out, thus contributing less to the batch expansion and hindering less the melting process than those evolving at later stages such as CO_2 when the interstitial channels start to close as the materials soften.[26]

Excessive gas evolution from GFCs was also observed in an earlier melting rate study in which batch chemicals were used in lieu of a pre-fabricated frit as the glass additives for a simulated PUREX SRAT product.[16] Foaming was so excessive during heating in the MRF that the tests were aborted. It was also found that excessive foaming persisted when lithium nitrate and sodium formate were used instead of lithium and sodium carbonate.

4.6 CT Calculated Densities versus Measured Densities

The material amounts in Table 4-4 were divided by the volume of each zone and the resulting CT calculated material densities are tabulated in Table 4-7. Of particular interest is how the material density of each melt zone correlates to the measured density of each fully-melted glass. As expected, the measured densities of high or low boron glasses were practically the same regardless of whether GFCs or frit was used. The measured densities of the low boron glasses were higher than those of the high boron glasses, which are also reflected by the calculated CT material densities. Variation of the material densities determined by CT of the high or low boron melt zones are likely due to: (1) the material in each melt zone was not homogeneous, i.e., it covered a range of CT densities, and (2) the melting characteristics of the GFCs-based feeds were different from those of the frit-based feeds.

Table 4-7. Comparison of Calculated CT Material Density and Measured Glass Density

Sample ID	Additive Form	CT Calculated Material Density (mm^{-3})			Measured Density (g/cm^3)
		Overall	Un-melted	Melt	Glass
High Boron					
MRF-14-39	Frit	11.29	9.49	16.99	2.60
MRF-14-14	GFCs	11.08	9.51	17.96	2.59
Low Boron					
MRF-14-07	Frit	12.93	10.38	19.15	2.67
MRF-14-19	GFCs	12.02	10.28	19.56	2.69

5.0 Conclusions

Two compositions of melter feeds based on the DWPF nitric-glycolic flowsheet SB6 SRAT product were studied in order to determine if differences in melting rate between frit and GFCs could be distinguished by the X-ray scanning and CT analysis technique. The glass additive compositions and WLs were defined by the PNNL 2009 and 2013 glass algorithms using the composition of the DWPF SB6 SRAT product. The 2009 algorithms yielded a high boron (low alkali) additive with a WL of 35.09% and the 2013 algorithms yielded a low boron (high alkali) additive with a WL of 39.22%. A total of 4 bench-scale melting rate tests were performed with the MRF and each resulting sample beaker was scanned with X-ray radially for a total of 360 radiographs per sample. Reconstruction of the sample data was performed using Imgrec software developed at LLNL to produce a 3D volumetric data set and histograms relating material amount and CT density were created, which differentiated the lower density un-melted material from the higher density melted material. In order to quantify the results, the amount of material in each of the un-melted and melted zones was calculated by determining the area under their respective CT histogram peaks. The following observations and conclusions were drawn from the results provided in this report:

- *High boron (low alkali) melter feed* - There are minimal or no differences between the melting rates of frit and GFCs.

- *Low boron (high alkali) melter feed* - The melting rate for the frit based melter feed is slightly higher than GFCs, which is most likely due to the additional CO_2 generation from the decomposition of Na_2CO_3 in the GFCs during melting.

- The evolution of excess CO_2 from the GFCs increases the total (calculated) gas evolution from the high and low boron feeds by 5% and 11% above those from the frit-based counterparts, respectively.

- The low boron feeds melted faster than their high boron counterparts despite the fact that the low boron melter feeds were based on a higher WL, which is likely due to the higher total sodium content (~64% more than the high boron feeds).

- All of the melting rate samples contained large voids between the melted and un-melted portions of the sample due to the high concentration of gas generators in these melter feed compositions as compared to the previous tests with the baseline nitric-formic acid melter feeds.

- The primary advantages of the X-ray CT technique are that it (i) eliminates subjectivity that was associated with the previous visual method, (ii) enables quantification of materials in varying

stages of melting along with the radial and vertical distribution of voids and bubbles, and (iii) allows for the entire volume of the sample to be analyzed as opposed to a 2D image of a particular cross-section, which may not be the most representative view of the entire sample.

6.0 Future Work

To meet the primary objective of this initial testing, once the pellet tests at PNNL have been completed, a thorough review of the data will be performed to determine if the results can be compared or provide complementary insight into the melting behavior of these different melter feeds. Since the melter

Other parameters influencing melting rate could also be studied using melter feeds that are more representative of WTP. SRNL and PNNL will jointly define the future scope, which may include the use of both MRF and pellet test platforms. Prior to future testing, it is desirable to repeat the MRF runs at varying heating time with accompanying gas analysis, which should provide further insight into (1) how the sample morphology and the gas evolution profiles change at different stages of heat treatment, and (2) identification of dominant reactions that occur at different stages of melting and correlating them to the observed sample morphology. As warranted, SRNL will develop the internal capability to perform the pellet test in support of the PNNL melting rate program.

While not discussed in this report, an additional 20 bench-scale melting rate tests were performed using two different reductants (formic versus glycolic acid) in a WL series of 32-44%. The melter feeds were fabricated with both frit and GFCs so that comparisons could be made to the results of this initial study. Total reconstruction of the 3D volumetric data sets could not be completed in time for inclusion in this report. Four replicates were also included in this data set, so there is more opportunity to better quantify the reproducibility and error associated with this technique. These results will be summarized in a separate report for DOE-ORP.

The potential for use of X-ray scanning and CT analysis could be expanded to include real-time scanning of samples during melting rate testing, which could supplement the post-test results. This technique has not yet been attempted, but it does seem to be feasible based on initial discussions and other previous applications of X-ray scanning performed at SRS. If reaction rates are significantly faster than X-ray scan rates, then this method may prove to be impractical.

7.0 References

1. P.J. Certa, R.D. Adams, G.K. Allen, J.D. Belsher, P.A. Empey, J.H. Foster, T.M. Hohl, R.T. Jasper, R.A. Kirkbride, R.L. Lytle, F.L. Meinert, J.S. Ritari, R.M. Russell, K.R. Seniow, E.B. West, M.N. Wells, and L.M. Bergmann, “River Protection Project System Plan,” Office of River Protection, Richland, WA, 11242, 2011.

2. J.D. Vienna, D.C. Skorski, D.S. Kim, and J. Matyáš, “Glass Property Models and Constraints for Estimating the Glass to Be Produced at Hanford by Implementing Current Advanced Glass Formulation Efforts,” Pacific Northwest National Laboratory, Richland, WA, EWG-RPT-003, 2013.

3. F.C. Johnson, A.S. Choi, and D.K. Peeler, “Task Technical and Quality Assurance Plan for the FY14 ORP Melt Rate Program,” Savannah River National Laboratory, Aiken, SC, SRNL-RP-2014-00439, 2014.

4. K.M. Fox and D.K. Peeler, “Task Technical and Quality Assurance Plan for Hanford HLW Glass Development and Characterization,” Savannah River National Laboratory, Aiken, SC, SRNL-RP-2013-00692, 2013.

5. T.H. Lorier and M.E. Smith, "Melt Rate Assessment of SB2/3 with Frit 418 - Effects of Waste Loading Acid Addition," Westinghouse Savannah River Company, Aiken, SC, WSRC-TR-2004-00098, 2004.

6. M.E. Stone and J.E. Josephs, "Melt Rate Improvement for DWPF MB3: Melt Rate Furnace Testing (U)," Westinghouse Savannah River Company, Aiken, SC, WSRC-TR-2001-00146, Revision 0, 2001.

7. D.K. Peeler, T.H. Lorier, D.F. Bickford, D.C. Witt, T.B. Edwards, K.G. Brown, I.A. Reamer, R.J. Workman, and J.D. Vienna, "Melt Rate Improvement for DWPF MB3: Frit Development and Model Assessment," Westinghouse Savannah River Company, Aiken, SC, WSRC-TR-2001-00131, 2001.

8. M.E. Smith, D.H. Miller, and T.M. Jones, "The Impact of the Source Alkali on Sludge Batch 3 Melt Rate," Savannah River National Laboratory, Aiken, SC, WSRC-TR-2005-00177, 2005.

9. M.E. Smith, A.B. Barnes, D.F. Bickford, and D.C. Iverson, "DWPF Melter Glass Pump Implementation and Design Improvement," pp. 171-8 in *Environmental Issues and Waste Management Technologies in the Ceramic and Nuclear Industries Xi.* John Wiley & Sons, Inc., 2006.

10. M.E. Smith and D.C. Iverson, "Installation of Bubblers in the Savannah River Site Defense Waste Processing Facility Melter," *Waste Management 2011 Proceedings,* (2011).

11. D.K. Peeler, T.H. Lorier, and J.D. Vienna, "Melt Rate Improvement for DWPF MB3: Foaming Theory and Mitigation Techniques," Savannah River National Laboratory, Aiken, SC, WSRC-RP-2001-00351, 2001.

12. S.K. Sundaram, W.E. Daniel Jr., P.P. Woskov, and J.S. Machuzak, "Cold-Cap Monitoring Using Millimeter-Wave Technology," in *Environmental Issues and Wate Management Technologies in the Ceramic and Nuclear Industries VII.* Edited by G.L. Smith, S.K. Sundaram, and R. Spearing. The American Ceramic Society, Westerville, OH, 2002.

13. D.S. Kim and P. Hrma, "Laboratory Studies for Estimation of Melting Rate in Nuclear Waste Glass Melters," pp. 409-19 in Vol. 45 (Ceramic Transactions), *Environmental and Waste Management Issues in the Ceramic Industry II.* Edited by D.F. Bickford, S. Bates, V. Jain, and G.L. Smith. 1994.

14. M.E. Stone and D.P. Lambert, "DWPF Macrobatch 2 Melt Rate Tests," Savannah River National Laboratory, Aiken, SC, WSRC-TR-2000-00395, 2000.

15. M.E. Stone and J.E. Josephs, "Melt Rate Improvement for DWPF MB3: Sugar Addition Test," Westinghouse Savannah River Company, Aiken,SC, WSRC-TR-2001-00158, 2001.

16. T.H. Lorier, T.M. Jones, and D.C. Witt, "Melt Rate Testing for the DWPF: Summary of FY02 Testing," Savannah River National Laboratory, Aiken, SC, WSRC-TR-2002-00545, 2002.

17. M.E. Smith, T.H. Lorier, and T.M. Jones, "SMRF and MRF DWPF Melt Rate Testing for SB2/SB3 (Case 6B-250 Canisters)," Westinghouse Savannah River Company, Aiken, SC, WSRC-TR-2003-00466, 2003.

18. D.H. Miller, M.E. Smith, and T.H. Lorier, "The Impact of Frit 202 on Melt Rate for the SB3 Feed System," Savannah River National Laboratory, Aiken, SC, WSRC-TR-2004-00453, 2004.

19. M.E. Smith and D.H. Miller, "Maximizing SB3 Waste Throughput Melt Rate Tests," Savannah River National Laboratory, Aiken, SC, WSRC-TR-2005-00456, 2005.

20. M.E. Smith, M.E. Stone, T.M. Jones, D.H. Miller, P.R. Burket, and D.M. Immel, "SB4 MRF and SMRF Tests with Frits 418, 425, and 503 (U)," Washington Savannah River Company, Aiken, SC, WSRC-STI-2006-00015, Revision 0, 2006.

21. M.E. Smith, T.M. Jones, and D.H. Miller, "Sludge Batch 4 Baseline Melt Rate Furnace and Slurry-Fed Melt Rate Furnace Tests with Frits 418 and 510," Savannah River National Laboratory, Aiken, SC, WSRC-STI-2007-00450, 2007.

22. D.H. Miller, K.M. Fox, B.R. Pickenheim, and M.E. Stone, "Melt Rate Furnace Testing for Sludge Batch 5 Frit Optimization," Savannah River National Laboratory, Aiken, SC, SRNS-STI-2008-00092, 2008.

23. D.H. Miller and B.R. Pickenheim, "Sludge Batch 5 Slurry Fed Melt Rate Furnace Tests with Frits 418 and 550," Savannah River National Laboratory, Aiken, SC, SRNL-STI-2008-00508, 2008.

24. K.M. Fox, D.H. Miller, and T.B. Edwards, "Preliminary Frit Development and Melt Rate Testing for Sludge Batch 6," Savannah River National Laboratory, Aiken, SC, SRNL-STI-2009-00440, 2009.

25. K.M. Fox, D.H. Miller, and B.R. Pickenheim, "Melt Rate Testing for Sludge Batch 6," Savannah River National Laboratory, Aiken, SC, SRNL-STI-2010-00230, 2010.

26. A.S. Choi, D.H. Miller, and D.M. Immel, "Determination of HLW Glass Melt Rate Using X-Ray Computed Tomography (CT)," Savannah River National Laboratory, Aiken, SC, SRNL-STI-2010-00767, 2010.

27. F.C. Johnson, M.E. Stone, and D.H. Miller, "Alternate Reductant Cold Cap Evaluation Furnace Phase II Testing," Savannah River National Laboratory, Aiken, SC, SRNL-STI-2014-00157, 2014.

28. D.P. Lambert, "Acceptance of Harrell Batch SB6I 100% Glycolic Nitric Acid Flowsheet SRAT Product," Savannah River National Laboratory, Aiken, SC, SRNL-L3100-2013-00118, 2013.

29. A.S. Choi, "DWPF Melter Off-Gas Flammability Model for the Nitric-Glycolic Acid Flowsheet," Savannah River National Laboratory, Aiken, SC, SRNL-STI-2014-00355, 2014.

30. J.D. Vienna, A. Fluegel, D.S. Kim, and P. Hrma, "Glass Property Data and Models for Estimating High-Level Wate Glass Volume," Pacific Northwest National Laboratory, Richland, WA, PNNL-18501, 2009.

31. R.F. Schumacher, "Characterization of HLW and Law Glass Formers," Westinghouse Savannah River Company, Aiken, SC, WSRC-TR-2002-00282, Rev. 1, 2003.

32. "Glass Batching," Savannah River National Laboratory, Aiken, SC, ITS-0001, current revision.

33. "Glass Melting," Savannah River National Laboratory, Aiken, SC, ITS-0003, current revision.

34. “Specification for Procurement of DWPF Glass Frit,” X-SPP-S-00018, current revision.

35. “Dissolution of Glass, Sludge and Slurry Samples Using Na_2O_2/NaOH/HCl,” Savannah River National Laboratory, Aiken, SC, ITS-0040, current revision.

36. “Lithium Metaborate Fusion Preparation,” Savannah River National Laboratory, Aiken, SC, ITS-0071, current revision.

37. “Inductively Coupled Plasma-Atomic Emission Spectrometer Agilent 730 ES,” Savannah River National Laboratory, Aiken, SC ITS-0079, current revision.

38. “Lithium Tetraborate Fusion Preparation,” Savannah River National Laboratory, Aiken, SC, ITS-0070, current revision.

39. “Glass Density Using the Mettler AT400 (or Equivalent) Balance,” Savannah River National Laboratory, Aiken, SC, ITS-0057, current revision.

40. A.S. Choi, “Validation of DWPF Melter Off-Gas Combustion Model,” Westinghouse Savannah River Company, Aiken, SC, WSRC-TR-2000-00100, 2000.

Distribution:

DOE-ORP
A.A. Kruger
P.R. Hrma

SRNL
S.L. Marra, 773-A
C.C. Herman, 773-A
D.H. McGuire, 999-W
E.N. Hoffman, 999-W
F.M. Pennebaker, 773-42A
S.D. Fink, 773-A
H.H. Burns, 773-41A
T.B. Brown, 773-A
R.L. Minichan, 781-A
W.R. Wilmarth, 773-A
J.W. Amoroso, 999-W
A.S. Choi, 999-W
J.H. Christian, 999-W
K.M. Fox, 999-W
F.C. Johnson, 999-W
K.A. Hill, 999-W
D.M. Immel, 781-A
D.H. Miller, 999-W
M.E. Stone, 999-W
M.S. Williams, 999-W

PNNL
M.J. Schweiger
J.D. Vienna
J. Matyáš
J.V. Crum

Records Administration (EDWS)